Environmental Microbiology

ENVIRONMENTAL MICROBIOLOGY

RESEARCH ARTICLE

Phytoplankton Exhibit Diverse Responses to Different Phases of Upwelling in the California Current System

Yuan Yu Lin[1] | Olivia Torano[1] | Emily Pierce[1,2] | Claire Till[3] | Matthew Hurst[3] | Astrid Schnetzer[2] | Harvey Seim[1] | Adrian Marchetti[1]

[1]Department of Earth, Marine, and Environmental Sciences, University of North Carolina, Chapel Hill, North Carolina, USA | [2]Department of Marine, Earth, and Atmospheric Sciences, North Carolina State University, Raleigh, North Carolina, USA | [3]Department of Chemistry, California State Polytechnic University, Humboldt, Arcata, California, USA

Correspondence: Adrian Marchetti (amarchetti@unc.edu)

Received: 13 January 2025 | **Revised:** 16 May 2025 | **Accepted:** 14 June 2025

Funding: This work was supported by National Science Foundation, OCE1751805; Research Corporation for Science Advancement, 26844.

Keywords: California current system | diatoms | metatranscriptomics | phytoplankton ecology | upwelling

ABSTRACT

Eastern boundary upwelling currents are some of the most biologically productive and diverse regions in the world's oceans. Driven by equatorward winds and Ekman transport, surface waters are transported offshore and replaced by cold, nutrient-rich deep waters that seed extensive phytoplankton blooms. Studying phytoplankton community succession and physiological acclimation during the initial stages of upwelling is critical to building a comprehensive understanding of phytoplankton responses to upwelling in these important regions. Additionally, factors like lateral transport, seed population dynamics and physiological and molecular shifts are conducive to shaping the community assemblage and primary productivity. This study examines how phytoplankton gene expression and resulting physiology change between early and later phases of upwelling. By incorporating metatranscriptomic analyses and stable isotope incubations to measure nutrient uptake kinetics into our assessment of early and later upwelling stages, we observed variability in phytoplankton assemblages and differential gene expression of phytoplankton that were de-coupled from their physiology. We show that the gene expression response to a fresh upwelling event precedes their physiological response. Ultimately, understanding how phytoplankton change through the course of an upwelling event is critical to assessing their importance to regional biological rate processes, trophic systems and resulting biogeochemistry.

1 | Introduction

The California current system (CCS) is defined by topographical, physical and biological diversity. Factors including atmospheric forcing, continental outflows, irregular coastlines and bathymetry fundamentally impact the direction and amplitude of coastal currents and water chemistry in the CCS (Bane et al. 2005; Checkley Jr and Barth 2009). In the summer, east-west pressure gradients created by the strengthening of the North Pacific High and deepening of the continental low form strong equatorward winds, and the resulting wind-driven Ekman transport lead to upwelling of nutrient-rich water near the coast (Checkley Jr and Barth 2009). Adding to the seasonality of this region are the complex physical patterns that may distribute the main California Current into smaller scale meanders, eddies, jets and filaments (Abbott and Zion 1987; Bernstein et al. 1977; Strub et al. 1991). Furthermore, these physical instabilities are compounded by the interactions between the alongshore flow and bottom bathymetric features (Narimousa and Maxworthy 1985).

From a biological standpoint, the wind-driven upwelling events during summer seasons can be viewed in the context of a conveyor belt, in which phytoplankton populations from the deep are carried by the direction of the upwelling plumes and

consequently transported offshore through Ekman transport as the upwelling water mass ages. In response, these phytoplankton acclimate to the different stages of the Upwelling Conveyor Belt Cycle through differential molecular and physiological strategies (Lampe et al. 2021; Lin et al. 2024). The biological succession of these upwelling plumes is often characterised by a substantial presence of diatoms, given their ability to respond rapidly to shifts in environmental conditions and utilise nitrate once brought into the euphotic zone. Diatoms have a documented ability to 'frontload' nitrogen assimilation genes more effectively than other phytoplankton functional groups prior to upwelling (Lampe et al. 2018, 2021; Lin et al. 2024). Barshis et al. (2013) coined the term 'frontload' as a mechanism by which corals constitutively highly express transcripts to maintain physiological resilience in the event of environmental stress. Similarly, frontloading is observed in large single-celled or chain-forming diatoms at depth (Lampe et al. 2018, 2021, Lin et al. 2024), allowing them to quickly acclimate to early upwelling stages with elevated nutrient conditions (Fawcett and Ward 2011) and contribute to a significant amount of new production and biomass accumulation in these eastern boundary upwelling systems (Bruland et al. 2001; Capone and Hutchins 2013). Yet the underpinning molecular and physiological changes in the various phytoplankton functional groups as the upwelling bloom ages remain largely uncharacterised. The community transitioning from early to later upwelling stages undergoes shifts in gene expression that are crucial to how they acclimate to the rapid environmental fluctuations as upwelling progresses. Such changes are likely to drive community succession as environmental conditions shift and species that can better take advantage of these limiting resources replace others (Valiela 1984).

Ultimately, identifying the transcriptional shifts within different phytoplankton taxa can help resolve the broader-level questions regarding phytoplankton community physiological status and succession. Previous studies have identified key diatom genes involved with their acclimation to early upwelling and adaptation to nutrient status. In particular, diatom genes related to nitrogen metabolism, polyamine biosynthesis and iron storage are often overrepresented under nutrient-replete conditions (Lin et al. 2024; Marchetti et al. 2012). In contrast, in oceanic high nutrient, low chlorophyll regions, diatom genes related to low iron availability (e.g., iron starvation-induced proteins) were overrepresented under iron-limited conditions (Marchetti et al. 2012). In the context of an upwelling plume, the expression of these genes is likely governed by resource availability between upwelling phases, when other phytoplankton taxa are also undergoing differential molecular shifts. The partitioning of gene expression at the taxonomic level has been documented in detail by previous field incubation and laboratory studies (Kolody et al. 2022; Lampe et al. 2018, 2021; Lin et al. 2024). But there have been limited studies investigating the key differences in phytoplankton molecular physiology within natural communities responding to the different stages of upwelling. Regions like the CCS provide a quintessential hotspot for biological production and carbon export. Evaluating the phytoplankton community dynamics along the ageing of an early upwelling plume will bolster our understanding of how biological rate processes and community compositional shifts in coastal oceans occur in both current and future ocean scenarios.

This study examines and compares the dynamics of phytoplankton blooms between the early and later stages of upwelling. We combine environmental, physiological and metatranscriptomic observations to examine phytoplankton community succession. In doing so, we postulate that the four stations sampled represent a mosaic of different stages of relatively early upwelling cycles such that they can be classified as either the initial onset of upwelling (early stage) in which the subsurface community only recently transitioned to the surface, or the relatively later phases (later stage) where the community has started to accumulate biomass and is undergoing the 'shift-up' response. This will potentially allow us to discern subtle environmental and biological differences even during the early stages of upwelling. We propose that (1) high variability of phytoplankton assemblages in the different upwelling stations is not fully representative of community succession, but rather of an aspect of the environmental forces that drive the biology of each particular station; (2) different phytoplankton groups exhibit divergent molecular and physiological responses that can be distinguished between initial upwelling and later upwelling stages regardless of macronutrient limitation; (3) there is an offset between gene expression and the physiological response in diatoms during these early phases of upwelling, where frontloading of N assimilation transcripts occurs before the 'shift-up' response is observed.

2 | Results

2.1 | Environmental Conditions and Upwelling Plume Characterisation

Initial observations based on remote sensing, conductivity, temperature and depth (CTD) casts and underway acoustic doppler current profiler (ADCP) data indicated that the four stations were located in distinct upwelling plumes (Figure 1),

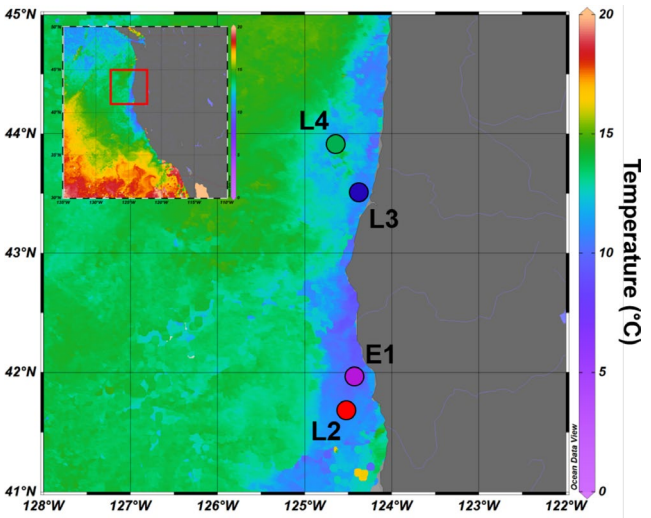

FIGURE 1 | Satellite-derived sea surface temperature (°C) map (8-day averages) depicting the early upwelling (E1) and late upwelling (L2, L3, and L4) stations during the time of collection. Stations E1 and L2 were sampled on May 30, 2019; stations L3 and L4 were sampled on June 5, 2019. Inset map indicates the larger study region of the CCS. Remote sensing data was derived from the NOAA CoastWatch programme and compiled using Ocean Data View.

with station E1 representing a relatively earlier stage of an upwelling event, while stations L2, L3 and L4 represented relatively later stages of upwelling that were still in the process of biomass accumulation (i.e., had not yet achieved peak phytoplankton biomass) and had not experienced nutrient limitation. Respective surface temperatures and salinity during the time of collection were 9.7°C and 33.8 PSU at E1 (5.7 m), 11.1°C and 32.8 PSU at L2 (5.7 m), 10.2°C and 32.9 PSU at L3 (5m), and 11.8°C and 32.6 PSU at L4 (5m). Stations E1 and L2 were identified as different water masses and not part of the same upwelling plume as indicated by their temperature-salinity characteristics, which showed a lower range of salinities at L2, and relatively higher salinity and lower temperatures at E1 (Figure 2). Furthermore, ADCP profiles indicated differences in the horizontal velocities of the water column as station E1 shifted to station L2 over the course of the day, where a sharp transition from a relatively indiscernible direction of flow at E1 shifted to a noticeable southward flow at L2 between 17:00 and 18:00 local time on May 29th.

Nitrate concentrations at station E1 were relatively high at all depths sampled, with a concentration of $12.9 \pm 3.2\,\mu mol\,L^{-1}$ near the surface, whereas concentrations at L2 were the lowest of all stations, with a near-surface concentration of $2.5 \pm 0.4\,\mu mol\,L^{-1}$ (Figure 3). Nitrate concentrations at stations L3 and L4 were comparably lower than those of station E1, although L3 had the second highest nitrate concentrations of the four sites. Similarly, phosphate and silicic acid

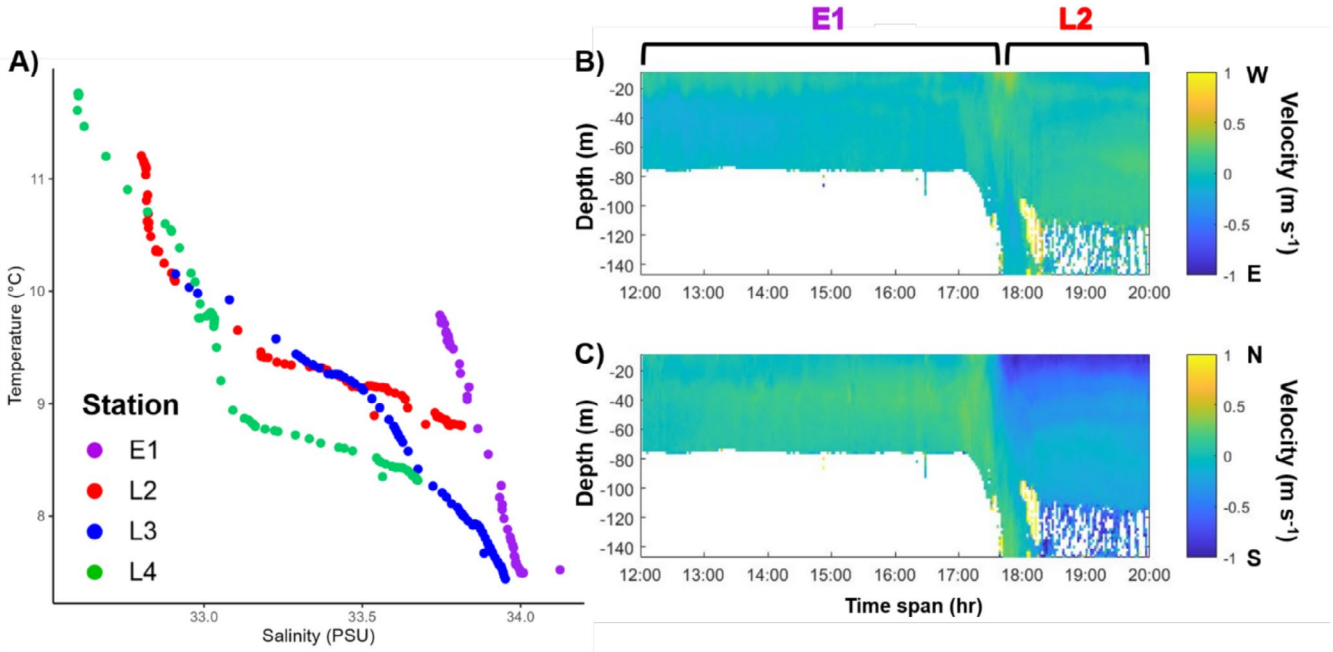

FIGURE 2 | Temperature-salinity plot (A) of the early upwelling station (E1) and the late upwelling stations (L2, L3 and L4) of the upper 75 m of the water column. The speed and direction of currents throughout the water column, as derived by shipboard ADCP data showcase horizontal velocities ($m\,s^{-1}$) in the (B) West to East (W/E) directions and (C) North to South (N/S) directions. Time increases from left to right as the ship transitions from station E1 to station L2 on the same day. The vertical axis depicts the depth in meters (negative values indicate distance from the surface) and represents the water column profile, where station E1 had a shallower depth of 74 m and L2 had a bottom depth of 417 m based on conductivity, temperature and depth (CTD) casts.

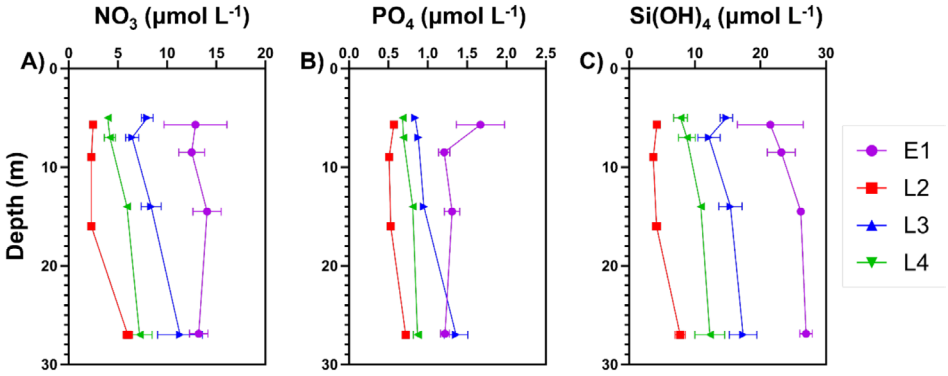

FIGURE 3 | Macronutrient concentrations ($\mu mol\,L^{-1}$) for nitrate (NO_3), phosphate (PO_4), and silicic acid ($Si(OH)_4$) in the respective upwelling transects (early upwelling station E1 and later upwelling stations L2, L3, and L4). Depths one through four correspond to approximately 5–6, 7–9, 14–16, and 27 m, respectively. Error bars represent the standard deviation of the mean ($n = 3$).

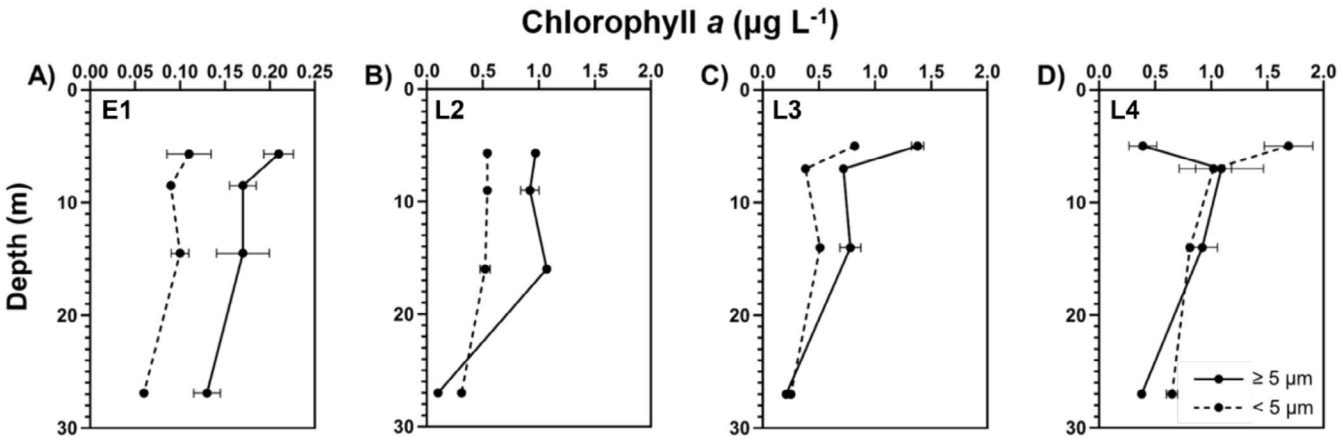

FIGURE 4 | Chlorophyll *a* concentrations ($\mu g\,L^{-1}$) of large cells ($\geq 5\,\mu m$) and small cells ($< 5\,\mu m$) sampled at the four depths for stations (A) E1, (B) L2, (C) L3 and (D) L4. Note the difference in scale between A and B–D. Error bars represent the standard deviation of the mean ($n = 3$).

concentrations were highest at E1, followed by stations L3, L4 and L2 (Figure 3). Both dissolved Fe (dFe, $< 0.2\,\mu m$ in size) and soluble Fe (sFe, $< 0.03\,\mu m$ in size) concentrations were generally higher at E1 relative to the later upwelling stations throughout the water column (Figure S1).

2.2 | Chlorophyll *a* Concentrations

Chlorophyll *a* (Chl *a*) concentrations of the large cell size fraction ($\geq 5\,\mu m$) throughout the euphotic zone at E1 were relatively lower than those of the later upwelling stations L2, L3, and L4 (Figure 4). The large size-fraction Chl *a* concentration in the surface waters ranged from $0.21 \pm 0.02\,mg\,L^{-1}$ to $1.38 \pm 0.06\,mg\,L^{-1}$ at station L3. Chl *a* concentrations in the smaller cell size fraction ($< 5\,\mu m$) were highest at L4 ($1.69 \pm 0.22\,\mu g\,L^{-1}$), which exceeded that of the larger cells in the near-surface at this station (Figure 4). This is followed by station L2 and station L3, in which the small cell populations comprised a fairly large proportion of the near-surface Chl *a* concentrations and were lowest at E1 ($0.11 \pm 0.02\,\mu g\,L^{-1}$).

2.3 | Absolute Uptake of Dissolved Inorganic Carbon and Nitrate

Absolute uptake rates of dissolved inorganic carbon (ρDIC) in the large cell size fraction ($\geq 5\,\mu m$) were relatively low at station E1 with near-surface rates of $146.48 \pm 17.10\,nmol\,L^{-1}$, but generally higher than those of the smaller cell ($< 5\,\mu m$) size fraction (Figure 5) with the exception of the community at 14.5 m. ρDIC in the larger cell size fraction at stations L2 and L3 was approximately 3-fold higher than those at station E1 and higher than those of the smaller cell size fraction at the surface, but there were no clear distinctions between the two size fractions below 5 m. At station L4, ρDIC in larger cells was generally lower than that of the smaller cells, with the exception of the rate at 7 m depth, which had the highest ρDIC of the large cell size fraction across all sites ($521.86 \pm 89.15\,nmol\,L^{-1}$) (Figure 5).

Absolute uptake rates of nitrate (NO_3^-) at station E1 were also low relative to the other stations in both the large cell and small cell size fractions (Figure 5). Rates in the near surface were 2.59 ± 0.38 and $1.37 \pm 0.34\,nmol\,L^{-1}$ in the large and small cells, respectively. Absolute nitrate uptake rates of large cells at stations L2 and L3 were 9 to 10-fold higher than at station E1 and higher than those of the small cells, especially in the shallowest surface waters. Trending similarly with ρDIC, absolute nitrate uptake rates at station L4 in larger cells were generally lower than those of the smaller cells, with the exception of the rate at 7 m depth, which had the highest NO_3^- uptake rate of the large cell size-fraction across all sites ($38.14 \pm 1.99\,nmol\,L^{-1}$).

2.4 | Biomass-Normalised Uptake of Dissolved Inorganic Carbon and Nitrate

At station E1, higher biomass-normalised dissolved inorganic carbon uptake rates (*V*DIC) were measured in the large cell size fraction than in the small cells at the two near-surface depths (5.7 and 8.5 m) (Figure 6). However, *V*DIC declined at deeper depths (14.5 and 26.9 m) and was nearly identical in both size fractions at E1 (Figure 6). Similarly, in the late upwelling stations, ~2-fold higher *V*DIC is observed in the shallower depths (5–6 and 7–9 m) for large cells at L2, L3 and L4 compared to station E1 and was generally higher than the small cells (Figure 6). Reduced *V*DIC is observed in both size fractions at the two deeper depths at all stations. For the large cell size fraction, biomass-normalised nitrate (VNO_3^-) uptake rates were lower at station E1 than at stations L2, L3, and L4 (Figure 6). Biomass-normalised VNO_3^- for the small cell size fraction is similarly low at station E1 relative to the later upwelling stations (Figure 6).

Ratios of ρDIC to ρNO_3^- were, on average, 3-fold higher at station E1 relative to the later upwelling stations (L2, L3 and L4) throughout all four depths of the euphotic zone (Figure 7). This was true for both cell size fractions. In all four stations, ρDIC:ρNO_3^- was relatively higher in the small cells compared to the large cells, suggesting lower nitrate uptake rates relative to that of DIC in the small phytoplankton population. This is also observed in the *V*DIC to VNO_3^-, which also indicates a relatively lower nitrate assimilation in both cell size fractions at station E1, such that the ratios are elevated relative to that of the

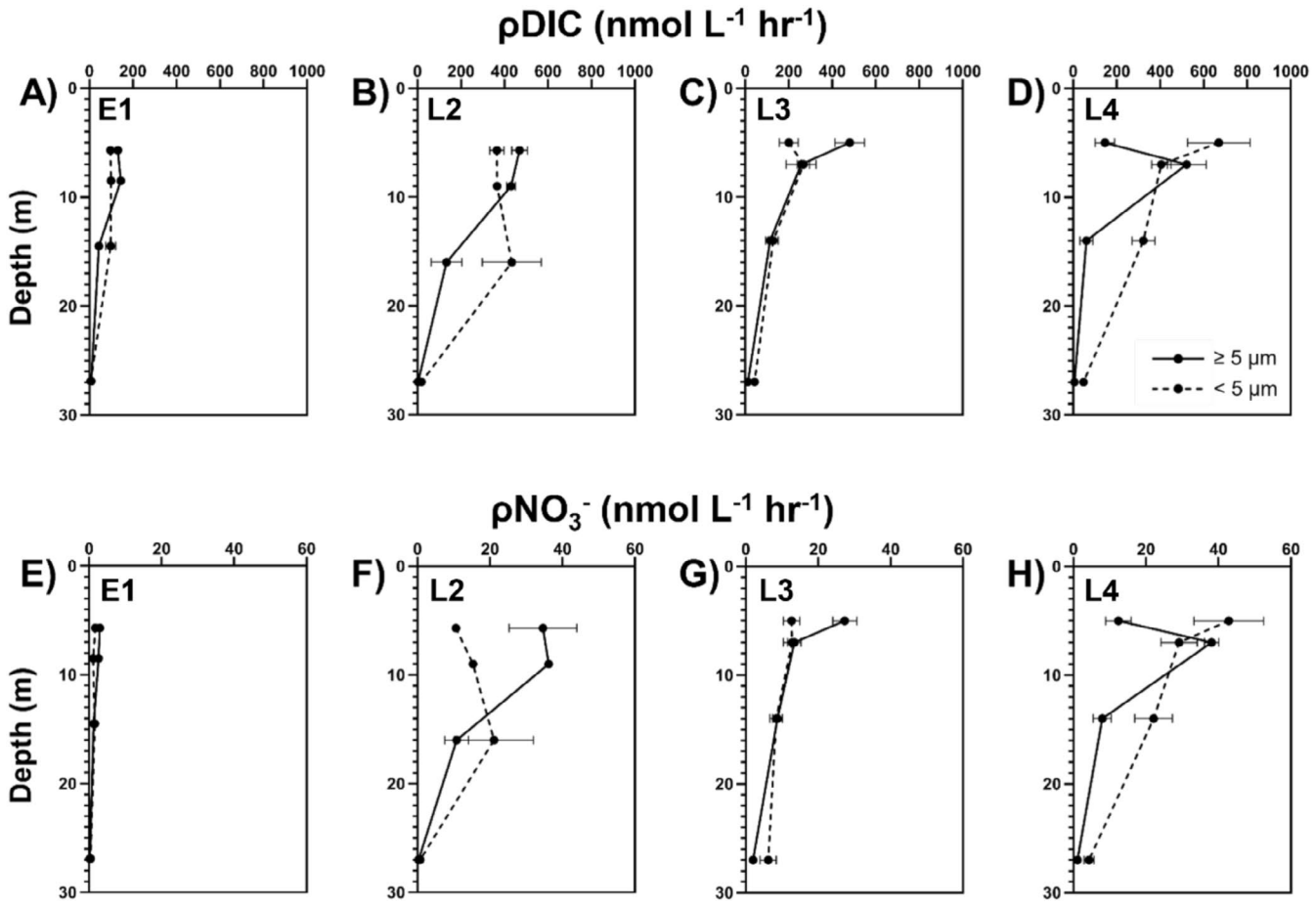

FIGURE 5 | Absolute uptake rates (nmol L^{-1} h^{-1}) of dissolved inorganic carbon (ρDIC) of large cells (≥ 5 µm) and small cells (< 5 µm) sampled at the four depths for stations (A) E1, (B) L2, (C) L3 and (D) L4. Absolute nitrate (ρNO_3^-) uptake rates of large cells (≥ 5 µm) and small cells (< 5 µm) were sampled at the four depths for stations (E) E1, (F) L2, (G) L3 and (H) L4. Error bars represent the standard deviation of the mean ($n = 3$).

Redfield ratio (~6.6) in this early upwelling station but lower in the later upwelling stations (L2, L3, and L4) for both size fractions (Figure 7).

2.5 | Principal Component Analysis

A principal component analysis (PCA) biplot (Figure S2) suggests close correlation of samples within station E1 that were distinctive from the other stations based on environmental and physiological parameters. The proportion of variance for the first principal component (PC1) was 57.18%, and it was 16.68% for the second principal component (PC2). Overall, the first two components explain over 70% of the variance among the four stations. Loading vectors suggest that environmental conditions such as macronutrient concentrations, salinity and temperature strongly influence the variability in PC1. There is also a positive correlation between macronutrient concentrations and salinity, which are negatively correlated to temperature. Biological variability influenced PC2, given that large size-fraction biomass, particulate organic material and uptake rates showed little correlation with the same parameters for the small size fraction.

2.6 | Phytoplankton Community Composition

Based on normalised transcript abundances, diatoms comprise over a third of the surface protist community at the early upwelling station E1 (39.5%), followed by chlorophytes (17.8%), dinoflagellates (16.0%) and haptophytes (10.2%). ciliophora (5.8%), cryptophytes (2.3%) and other taxa (8.3%) made up the rest of the protist community (Figure 8). Similarly, diatom transcript abundances were largest at station L3 (37.4%), followed by those of chlorophytes (15.4%), haptophytes (12.7%), ciliophora (12.2%) dinoflagellates (9.6%), cryptophytes (2.7%) and other phytoplankton (10.0%). At stations L2 and L4, a more even distribution of transcriptional activity for protist taxa was observed among diatoms (L2: 22.8%, L4: 22.0%), chlorophytes (L2: 25.5%, L4: 27.0%), dinoflagellates (L2: 14.5%, L4: 11.9%), haptophytes (L2: 13.2%, L4: 16.4%) and ciliophora (L2: 12.4%, L4: 13.7%). Cryptophytes (L2: 3.6%, L4: 1.7%) and other taxa (L2: 8.0%, L4: 7.3%) transcript abundances made up the rest of the protist community (Figure 8). Based on particle counts measured by a FlowCam, diatom abundances were relatively lower at station E1 than at the later stations (L2, L3, and L4). The early upwelling community consisted of a fairly large number of *Thalassiosira*, followed by *Pseudo-nitzschia*,

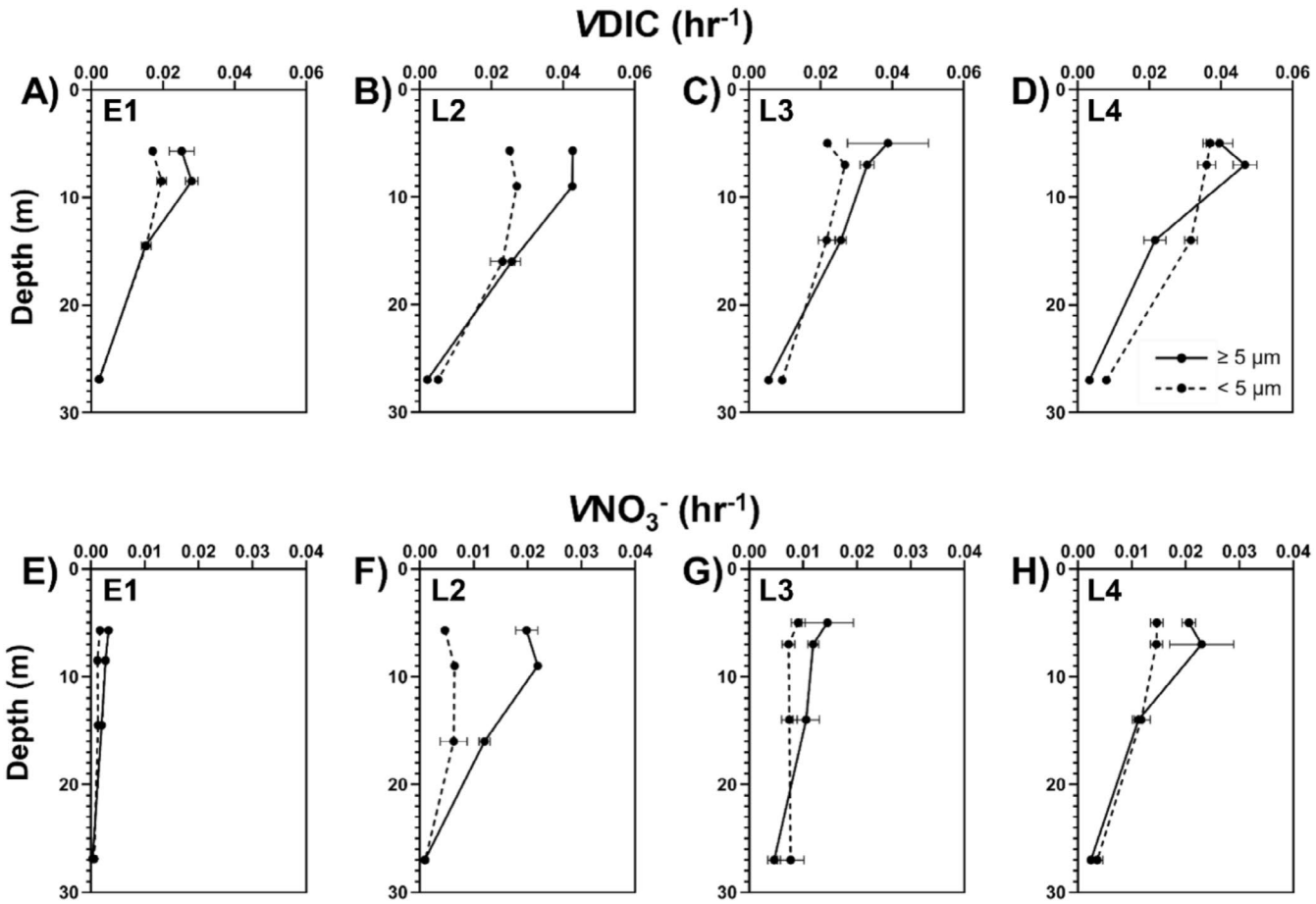

FIGURE 6 | Biomass-normalised dissolved inorganic carbon (*V*DIC) uptake rates (h^{-1}) of large cells (≥ 5 µm) and small cells (< 5 µm) sampled at the four depths for stations (A) E1, (B) L2, (C) L3 and (D) L4. Biomass-normalised nitrate (VNO_3^-) uptake rates of large cells (≥ 5 µm) and small cells (< 5 µm) were sampled at the four depths for stations (E) E1, (F) L2, (G) L3, and (H) L4. Values were normalised to particulate carbon or nitrogen concentrations in the samples. Error bars represent the standard deviation of the mean ($n = 3$).

Skeletonema, *Dictyocha* and *Asterionellopsis* (Figure S3). At stations L2 and L3, a large presence of *Chaetoceros* species was found in the upwelling plumes, as well as *Thalassiosira*, *Skeletonema* and *Pseudo-nitzschia* (for station L2). Station L4 consisted of a large number of the pennate diatoms *Pseudo-nitzschia* and *Nitzschia* (Figure S3).

2.7 | Gene Expression in the Phytoplankton Community

At the community level, both chlorophytes and haptophytes displayed differential gene expression responses in contrast to diatoms and dinoflagellates. Genes related to nitrogen metabolism, DNA polymerase, proteasome, protein processing, repair and replication systems were highly expressed in the later upwelling stages relative to the early upwelling stage in chlorophytes and haptophytes (Figure 8). Diatoms in the early upwelling station E1 exhibited higher expression (positive $\log_2$ of the fold change) of genes related to environmental information processing, iron storage, nitrogen metabolism, polyamine biosynthesis and replication system relative to diatoms in the later upwelling stations (average of L2, L3 and L4) (Figure 8). Diatoms and dinoflagellates were the only major phytoplankton taxa observed to show differential expression of genes related to environmental information processing, where genes corresponding to transport systems for metallic cation, iron-siderophore, vitamin B_{12}, phosphate, amino acid, saccharide, polyol and lipid were all highly expressed in the early upwelling station relative to the later upwelling stations (Figure 8).

In diatoms, the gene encoding for ferritin (*FTN*), nitrogen metabolism genes such as nitrogen transporters (*NRT*), nitrate reductases (*NR*) and ferredoxin nitrite reductases (*nirA*), and urea cycle genes such as argininosuccinate synthase (*argG*) and carbamoyl-phosphate synthase (*CPS1*) were significantly overrepresented ($p\text{adj} < 0.05$) at E1 compared to the later upwelling stages (Figure 9). Inversely, aldolases (*ALDO*), ferredoxin sulphite reductases and the iron-starvation-induced proteins (*pTF, formerly ISIP2a;* and *ISIP3*, McQuaid et al. 2018) were significantly overrepresented ($p\text{adj} < 0.05$) in the later upwelling stations relative to the early upwelling station E1 (Figure 9). Furthermore, the gene encoding replication protein A14 kDa subunit (*RPA3*) was also significantly overrepresented in diatoms at E1 than in the later upwelling stations. In dinoflagellates and chlorophytes, no clear significance can be attributed to the differential expression of nitrogen metabolism and *ISIP*s between the early and later upwelling stages, but *RPA3* is highly expressed at the later upwelling stages

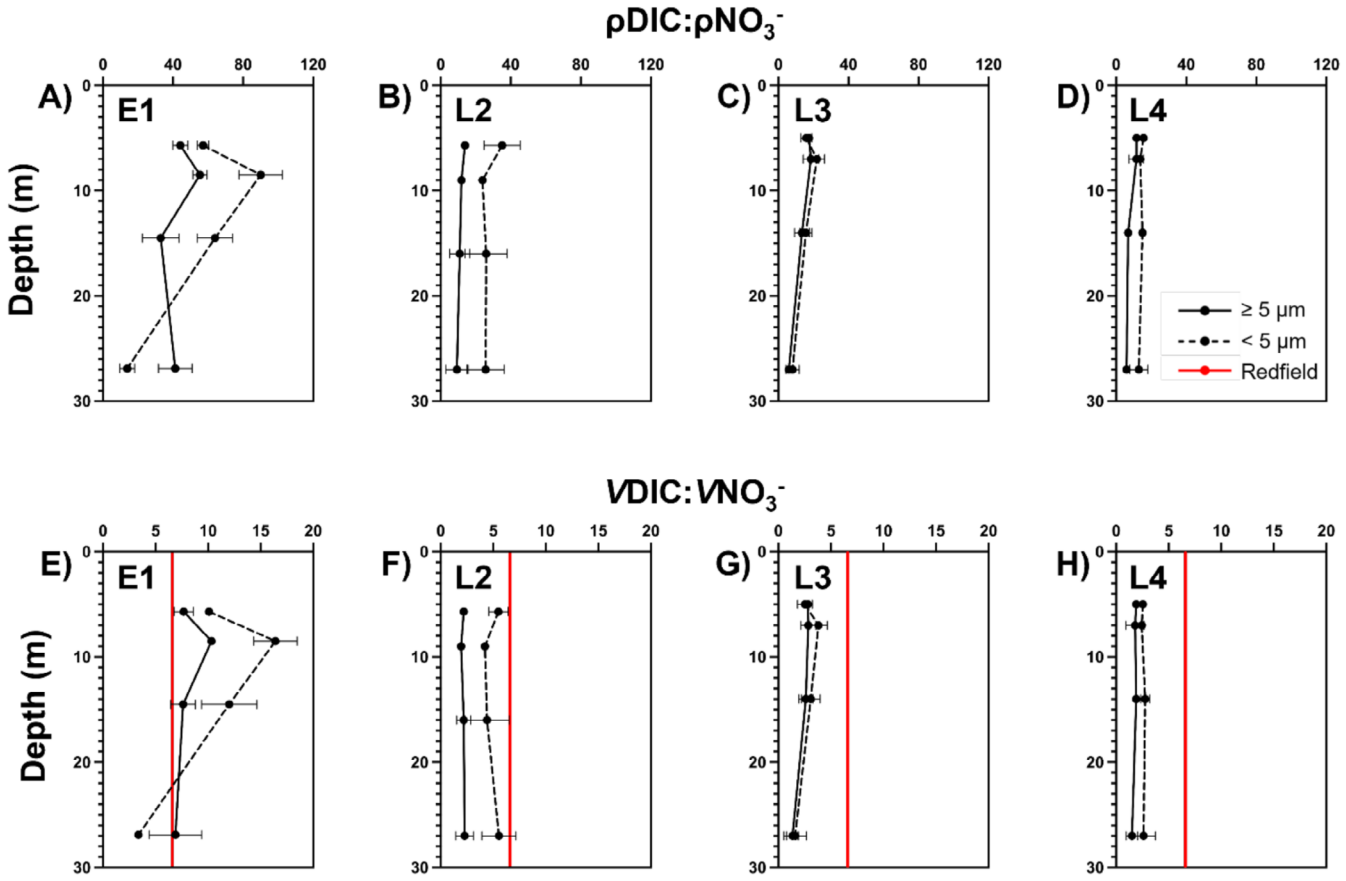

FIGURE 7 | Absolute dissolved inorganic carbon (ρDIC) to nitrate (ρNO_3^-) uptake ratios of large cells (≥ 5 µm) and small cells (< 5 µm) sampled at the four depths for stations (A) E1, (B) L2, (C) L3 and (D) L4. Biomass-normalised dissolved inorganic carbon (*V*DIC) to nitrate (VNO_3^-) uptake ratios of large cells (≥ 5 µm) and small cells (< 5 µm) sampled at the four depths for stations (E) E1, (F) L2, (G) L3 and (H) L4. Red lines indicate the canonical Redfield ratio for phytoplankton elemental stoichiometry (Redfield et al. 1963). Error bars represent the standard deviation of the mean ($n = 3$).

than at E1. *ISIPs* and aldolases (*ALDO*) in haptophytes, and fructose bisphosphate aldolase (*FBA*) in both chlorophytes and haptophytes were found to be overrepresented in the early upwelling stages (Figure 9). Differential gene expression among the four taxa can also be observed in proton-pumping rhodopsins (*RHO*), which are overrepresented in diatoms in the later upwelling stations, but vice versa in dinoflagellates and haptophytes, respectively.

3 | Discussion

3.1 | Environmental Data

The satellite-derived surface temperature data (Figure 1) depict four distinct upwelling sites sampled along the California coast. Station E1 represents the relatively earlier stage of an upwelling cycle, while stations L2, L3 and L4 represent relatively later stages. Temperature-salinity (TS) characteristics were used to highlight the distinctions in water properties between E1 and the later upwelling stations, where relatively higher salinity, narrower salinity ranges and low temperatures are distinctive from the later upwelling stations with a wider range of salinities and higher temperatures. Fresh water inputs from these regions may have contributed to the wider range and lower values of salinity compared to the early upwelling station. Stations E1 and L2 were originally thought to have been part of the same upwelling filament but were subsequently classified as two separate upwelling water masses, albeit at different stages. This was determined by examining the ADCP data, which displayed differential horizontal velocities and flow directions of the water column between stations E1 and L2 over the course of the day. The noticeable change from a relatively inappreciable current direction at station E1 to an apparent southward flow at L2 suggests the two respective water masses were heading in different directions throughout the upper 75 m as the ship transitioned from station E1 to L2 on May 30th. Additionally, environmental parameters suggest a clear distinction at station E1 relative to the other upwelling stations, as depicted by the PCA. Concentrations of these macronutrients at E1 were also higher relative to the other three stations, where nutrient drawdown may have occurred at the later stages of the respective upwelling plumes. However, there is no evidence to suggest a direct causation between the build-up of biomass and the macronutrient drawdown. Physical forces like lateral transport (Gruber et al. 2011) may have brought in low-nutrient waters from another region and diluted the macronutrient concentrations for any of the upwelling stations. Furthermore, the relatively low NO_3^-:PO_4 ratios throughout the four sites provide evidence that the upwelled water in the CCS contains lower amounts of dissolved NO_3^- due to its age and hypoxic conditions (Capone and Hutchins 2013). Both dissolved Fe and soluble Fe were relatively higher at E1 than at the later upwelling stations (Figure S1), and substantially increased in concentration towards the bottom of the euphotic zone at station

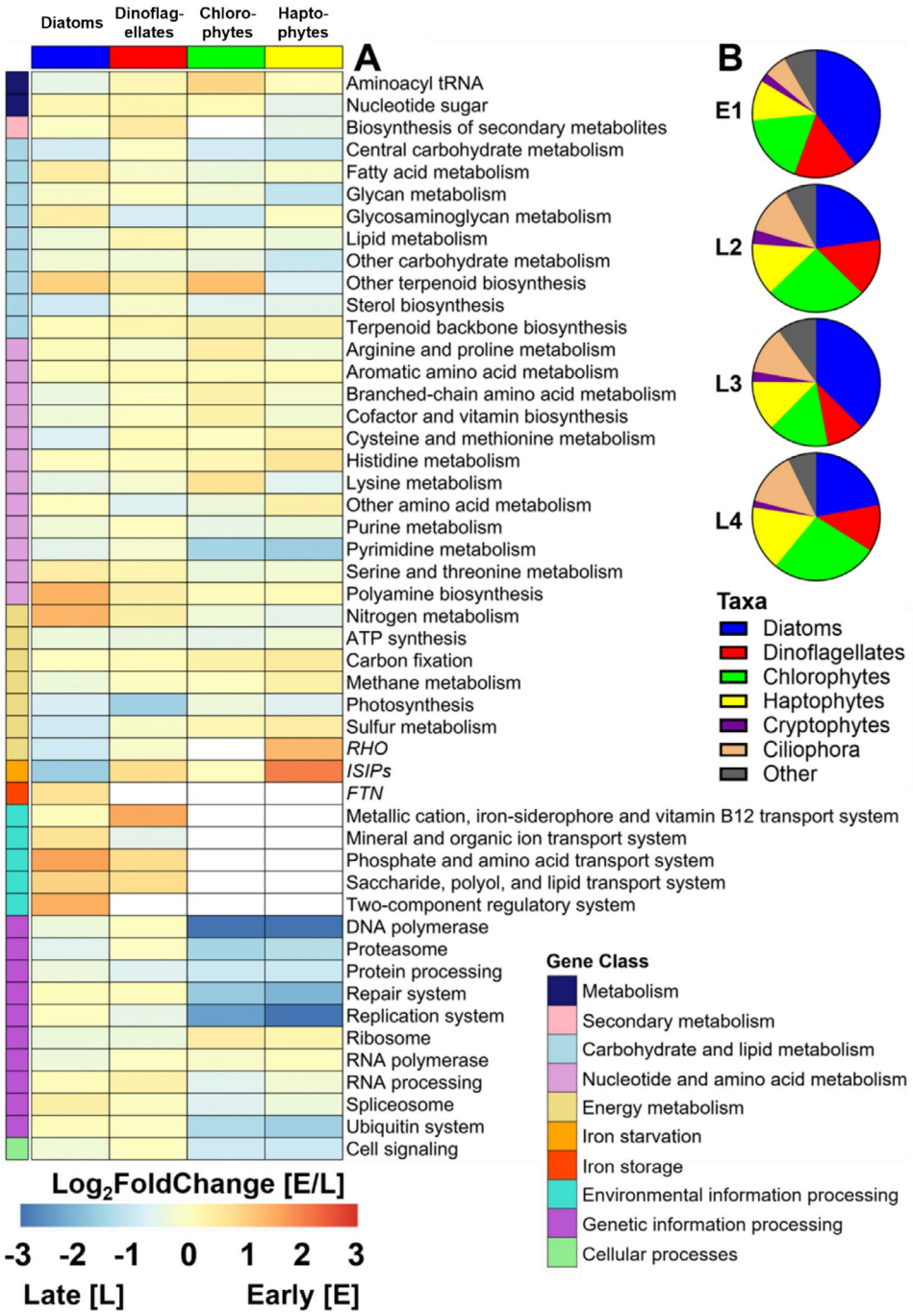

FIGURE 8 | (A) Heatmap depicting differential expression of Class II (Gene Class) and Class III level pathways (assigned by KEGG modules) among the four major phytoplankton taxa (diatoms, dinoflagellates, chlorophytes and haptophytes) as depicted by the Log_2FoldChange between early (E1) and late (L2, L3, L4) upwelling stages. Proton-pumping rhodopsins (*RHO*), iron starvation-induced proteins (*ISIPs*) and ferritin (*FTN*) are also displayed as differentially expressed genes between early and late upwelling stages. White boxes represent genes that were not mapped or did not exhibit differential expression in the respective taxa. (B) Pie charts depicting average taxonomic distributions by normalised mapped reads (RNA transcripts) from each upwelling site (E1, L2, L3, L4). Taxonomic distributions are categorised as percentage of mapped reads from the whole phytoplankton community.

E1, likely due to a sedimentary source of dFe and sFe to the water column during upwelling events at the early upwelling site (Biller and Bruland 2013). However, dFe can also be released from the degradation of organic matter in the water column, which may have led to the bottom water dFe maxima observed in our measurements (Klar et al. 2017).

3.2 | Primary Productivity Data

As a proxy for phytoplankton biomass estimates, chlorophyll *a* concentrations for the four upwelling stations portray a similar story of the separation of two different upwelling stages. The lower phytoplankton biomass in both size fractions of station

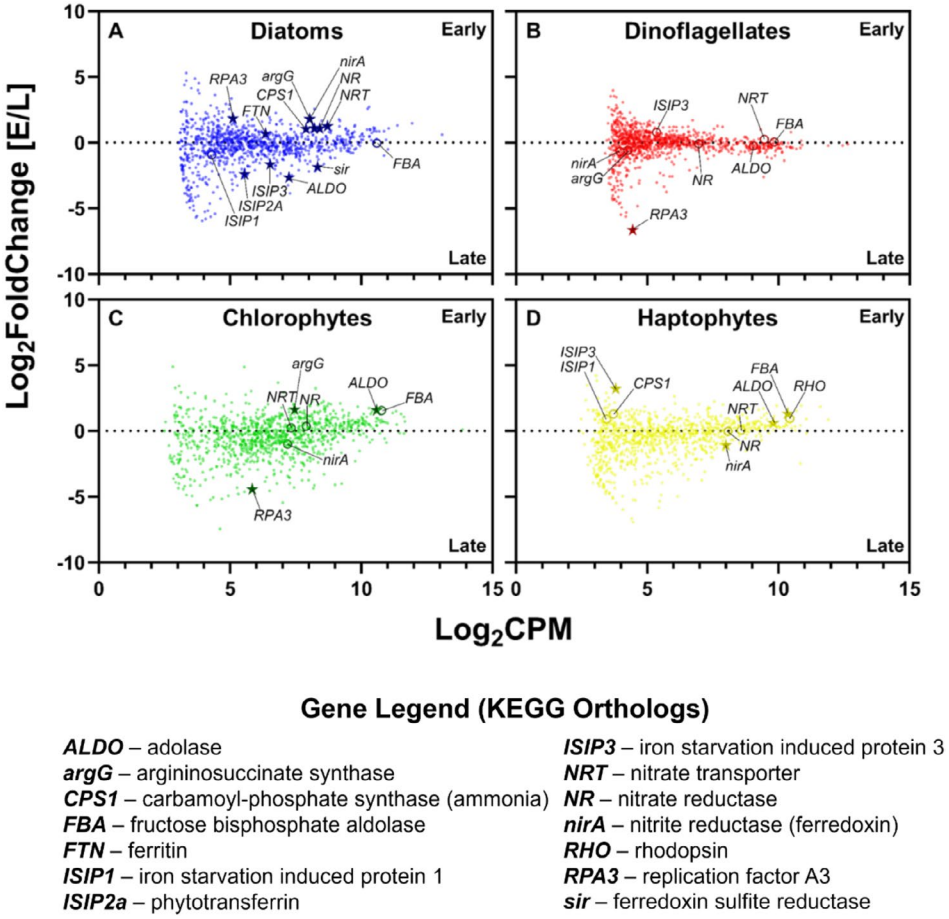

Gene Legend (KEGG Orthologs)

ALDO – adolase	***ISIP3*** – iron starvation induced protein 3
argG – argininosuccinate synthase	***NRT*** – nitrate transporter
CPS1 – carbamoyl-phosphate synthase (ammonia)	***NR*** – nitrate reductase
FBA – fructose bisphosphate aldolase	***nirA*** – nitrite reductase (ferredoxin)
FTN – ferritin	***RHO*** – rhodopsin
ISIP1 – iron starvation induced protein 1	***RPA3*** – replication factor A3
ISIP2a – phytotransferrin	***sir*** – ferredoxin sulfite reductase

FIGURE 9 | Differentially expressed mapped genes between early (E1) and late (L2, L3, L4, grouped) upwelling stages in (A) diatoms, (B) dinoflagellates, (C) chlorophytes and (D) haptophytes. Plotted is the Log_2 of the counts per million of each gene versus the log_2 fold change of genes at the early versus later stage upwelling stations. Stars represent significantly differentially expressed genes (p-adj < 0.05).

E1 is consistent with environmental data in that the populations present in these waters were still acclimating to the early stages of the upwelling plume. Chl *a* concentrations in the larger size fraction of the later upwelling stages (L2-L4) were close to an order of magnitude higher than those of E1, indicating enhanced biomass accumulation as the early upwelling stage transitioned to that of a later one. Previous studies have shown that biomass increases in larger phytoplankton are disproportionally higher than that of smaller phytoplankton under high resource conditions (Goericke 2011; Poulin and Franks 2010). Larger diatoms are especially proficient in exploiting higher nutrient conditions compared to other smaller phytoplankton species, whose growth rates saturate at lower nutrient and light levels (Barber and Hiscock 2006; Litchman et al. 2007).

The observably high ratios of absolute dissolved inorganic carbon uptake to dissolved inorganic nitrogen uptake rates can be attributed to the uncoupling of DIC to NO_3^- uptake measurements with respect to the day/night cycle. The 6-h incubations only captured a snapshot in time for when cells were actively taking up both DIC and NO_3^- under ambient light conditions, but did not take into account the lack of DIC assimilation during night time. Ultimately this may have contributed to an overestimate of DIC uptake rates relative to NO_3^- uptake rates. As a general interpretation, however, size-fractionated absolute uptake rates of carbon and nitrogen corresponded to that of chlorophyll *a* data in all four stations, as the relatively lower particulate organic carbon (POC) and biomass at E1 likely resulted from lower absolute uptake rates by the community. The same patterns are observed for the absolute nitrate uptake rates at E1, which were close to an order of magnitude lower than at L2 and L3. We also observed higher uptake rates in the large cell size fraction of the near surface waters at E1, L2 and L3, indicating the possibility that the larger-sized diatoms may be contributing a significant portion of nutrient uptake at the three sites. The diminished large size-fraction phytoplankton biomass and uptake rates in the near-surface waters of L4 coincides with enhanced rates of the smaller phytoplankton community, which either may have had a larger subsurface population prior to upwelling or were the dominant groups found in the region given station L4's further distance from the coast. In the latter scenario, lower entrainment of Fe due to deeper waters and diminished proximity to freshwater iron sources may explain this trend, where small cells are typically well adapted to lower nutrient regimes (Barber and Hiscock 2006, Litchman et al. 2007). Furthermore, FlowCam-derived cell counts suggests a heavy presence of the pennate diatoms such as *Pseudo-nitzschia* and *Nitzschia*, which may have passed through the 5 μm polycarbonate membranes during bulk-size fractionation due to their needle-like morphology. In such cases, these smaller diatoms were measured as part of the small cell community and could have contributed to the small-cell biomass and uptake rates as indicated in our

physiological data. Alternatively, top-down controls (Mozetič et al. 2012) and efficient sinking of the large cell population (Pitcher et al. 1991; Inoue and Taniguichi 1999) might have also contributed to the difference found at L4.

Biomass-normalised uptake rates of carbon and nitrogen present a more accurate depiction of the nutrient assimilation for each station and were also consistent with that of the chlorophyll *a* data. Phytoplankton at E1 displayed relatively lower rates compared to their counterparts in L2, L3 and L4, suggesting that the community has yet to undergo the shift-up response to upwelling at station E1. Both absolute and biomass-normalised DIC to nitrate uptake ratios further suggest the relatively lower nitrogen assimilation rates of the phytoplankton community at the early upwelling station (E1). Indeed, normalised carbon to nitrogen uptake ratios at E1 were higher than that of the Redfield ratio (Redfield et al. 1963), while the reverse was true for the later upwelling stations (L2, L3, and L4). This indicates that cells of both size fractions at E1 were not assimilating nitrogen at as high rates as cells at L2, L3 and L4, where they were probably accelerating nitrogen uptake relative to carbon uptake to build up cellular machinery, divide, and accumulate biomass (Dugdale et al. 1990; Fawcett and Ward 2011; Wilkerson and Dugdale 1987). One possible explanation for this discrepancy between cells in the early and later upwelling stages is the temporal lag between the response at the gene-expression level and the physiological response of the cell (Collos 1986; Van Oostende et al. 2015). Influenced by both the physiological status and the scale of the environmental shift, cells exposed to rapid increases in nutrient concentrations will often exhibit a time lag in growth and acclimation to their new environmental conditions (Collos 1986; Collos et al. 2005; Van Oostende et al. 2015).

Overall, the physical, chemical and biological properties of the upwelling stations present evidence that station E1 was distinct from the other stations, where it was still in the initial stages of upwelling as the algal community had yet to accumulate enough biomass to exhibit the 'shift-up' response on the physiological level. While there was macronutrient drawdown at the later upwelling stations (L2, L3 and L4), it was not considered to be at the point of limiting nutrient concentrations. The biomass accumulation at these later stations also did not reach the point of a late-stage bloom, and along with our physiological measurements, phytoplankton at these sites were still undergoing the 'shift-up' response. In essence, all four upwelling stations may still have been in early to mid-stage phases of the upwelling cycle, with station E1 being the earliest. Our findings from the environmental and physiological data allow for a closer examination of the phytoplankton community composition and gene expression, and how they might differ between the early and later upwelling stages.

3.3 | Phytoplankton Community Composition and Module Level Expression

Community composition based on normalised transcripts suggests that diatom transcriptional activity is high at station E1 and L3. Transcript abundances at stations L2 and L4 follow a more even distribution among the phytoplankton taxa. Nonetheless, inferences of community succession cannot be made using data collected from these four sites, as they represent differing upwelling stations influenced by differing environmental factors.

Based on previous field experiments, taxonomic diversity seems to increase over the course of an upwelling plume despite a decline in nitrate concentrations (Fawcett and Ward 2011). This may be attributed to either an increase in the number of species entrained into the upwelled waters or an increase in the evenness of the community (Fawcett and Ward 2011).

Differential gene expression is observed among the four major phytoplankton taxa (diatoms, dinoflagellates, chlorophytes and haptophytes); chlorophyte and haptophyte gene expression largely contrast with those of diatoms in the context of early and later upwelling. Only diatoms and dinoflagellates seem to express genes related to environmental information processing, suggesting these phytoplankton groups seem to perceive environmental shifts by 'sensing' their environmental cues (Jaubert et al. 2022). Genes related to nitrogen metabolism and replication and repair systems are overrepresented in haptophytes and chlorophytes but underrepresented in diatoms and dinoflagellates at the later upwelling stages, while the reverse is true for the early upwelling stage. It has been postulated that haptophytes like *Phaeocystis* are particularly adapted to iron limitation in the Southern Ocean and would prefer to increase nitrate assimilation under low iron availability to support colonial growth (Rizkallah et al. 2020; Wang et al. 2011). Interestingly, ISIP transcripts were found to be significantly overrepresented in early upwelling haptophytes relative to their later upwelling counterparts despite previous studies suggesting that the genes encoding these Fe acquisition proteins are constitutively expressed within these phytoplankton rather than being a part of iron sensing or regulatory response pathways (Bender et al. 2018). The differential expression of genetic information processing transcripts among the four major phytoplankton taxa are also notable in our interpretation of the upwelling succession, suggesting that chlorophytes and haptophytes are undergoing enhanced transcription at the later upwelling stages. These small-celled late survivors, such as the haptophytes *Gephyrocapsa huxleyi* (Botebol et al. 2017) and *Phaeocystis antarctica* (Bender et al. 2018; Strzepek et al. 2011), and chlorophyte strains of *Bathycoccus* and *Ostreococcus*, seem to exhibit lower iron requirements and possess various iron acquisition strategies that enable their survival in chronically low iron waters (Bender et al. 2018; Botebol et al. 2017). Nonetheless, none of the later upwelling stations seemed to be nutrient limited (e.g., by nitrate or iron), so the high expression of transcripts for ISIPs and aldolases in the smaller-celled haptophytes indicate not only a more reactive approach to their upwelling response but also a potential ability to frontload these genes as a metabolic strategy to prime themselves to nutrient-deplete conditions during the later stages of upwelling.

3.4 | Diatom Gene Expression

In diatoms, higher expression of genes related to nitrogen metabolism, iron storage, polyamine biosynthesis and replication system can be observed at station E1 when compared to the average of the later upwelling stations (L2, L3 and L4), where these gene groups are underrepresented. Diatoms have

an innate ability to take advantage of high nutrient concentrations and proactively assimilate nitrate before the other major phytoplankton taxa can react at an early upwelling stage, a strategy described previously as gene frontloading (Lampe et al. 2018). Yet, the overrepresentation of these transcripts contradicts our findings at the physiological level, where nitrate assimilation seems to be highest at the later upwelling stages. This may be attributed to the progression from initial transcriptional activity in subsurface seed populations that offset the delayed physiological response in the relatively later upwelling stages. The higher representation of diatom ferritin transcripts at this early upwelling stage further links iron to nitrogen metabolism, as the diatoms utilise the iron concentrating protein to safely store iron when it is more readily available (Marchetti et al. 2009). Interestingly, the high expression of diatom nitrogen metabolism genes coincides with the high expression of urea cycle genes during early upwelling. Carbamoyl-phosphate synthase (*CPS*) and argininosuccinate synthase (*argG*) were both found to be significantly highly expressed in diatoms at E1 compared to the diatoms at the later upwelling stations. It is likely that these urea cycle genes play a vital role in encoding proteins used in the storage and recycling of nitrogen, where CPS is found to facilitate the reallocation of inorganic carbon and nitrogen from catabolic metabolism and influence the synthesis of proline and glutamine, metabolites critical for diatom cell wall formation and cellular nitrogen status (Allen et al. 2011).

During the later upwelling stages, the higher expression of genes related to sulphur metabolism, aldolases and ISIPs in diatoms is a stark contrast to their early upwelling counterparts and further evidence of the offset between molecular and physiological processes. The increased transcription of sulphur metabolism genes like ferredoxin sulphite reductase often suggests correlation with nitrogen limitation, which inhibits diatom biomass production and increases organic carbon and sulphur excretion (van Tol and Armbrust 2021). In essence, sulphur metabolism is often found to replace nitrogen metabolism under nutrient-limiting conditions (van Tol and Armbrust 2021). Yet, none of the three later upwelling stations were observed to be depleted of nitrate, so the overrepresentation of sulphur metabolism transcripts in the later upwelling stages may not be due to nutrient limitation.

Previous studies examining the iron status of diatoms observed similar increased expression patterns of iron acquisition proteins under low iron conditions. In particular, phytotransferrin (*pTF*), which binds iron at the cell surface, is thought to be involved in intracellular iron transport for diatoms under iron-stressed conditions (Cohen et al. 2017; McQuaid et al. 2018; Morrissey et al. 2015). In contrast, our study presents evidence that diatoms expressing ISIP transcripts are overrepresented in the later upwelling sites before it appears that iron is likely limiting (Figure S1). This overrepresentation of ISIP transcripts may suggest the possibility that diatoms may be experiencing a certain level of iron stress, perhaps due to limited availability through iron complexation. Other phytoplankton groups exhibited overrepresentation of ISIPs at the early station, highlighting a differential response among phytoplankton groups. They may be proactively transcribing these genes to help acclimate to the onset of iron limitation, or perhaps they are constitutively expressing them, as observed in haptophytes (Bender et al. 2018). In diatoms, certain aldolase genes are also expressed highly under iron limitation and are responsible for both the synthesis and mobilisation of storage molecules at the onset of light and nutrient limitation (Allen et al. 2012). Evidence for the potential frontloading and coupling of ISIP and aldolase transcripts should be further examined in the context of phytoplankton upwelling succession in coastal systems. There is also the likelihood that other environmental factors may have influenced their gene expression.

Our combined metatranscriptomic analysis coupled with physiology measurements demonstrates how gene expression precedes phenotypic response. It is likely that the larger cells at E1 were still acclimating to the initial onset of upwelling, but did not undergo a 'shift-up' response in which they were yet to assimilate nitrate at a higher rate than that of carbon. In contrast, diatoms at this station seem to exhibit high transcription of nitrogen assimilation genes. For the later stations, while the high large cell chlorophyll *a* concentrations and nitrate uptake rates suggest a 'shift-up' response, diatoms seem to be ramping down nitrogen assimilation gene expression during these 'later' stages relative to their 'early' stage. This sampling of two upwelling stages highlights a potential decoupling between molecular level and physiological processes in large cells during the early stages of upwelling. However, given that size-fractionated physiology data does not possess the same level of taxonomic resolution as our molecular measurements, there is room for advancement in our approach to pairing gene expression with biological rate processes, such as through using fluorescence-assisted cell sorting techniques to quantify taxonomically resolved nutrient uptake rates.

4 | Conclusions

A combination of physiological and gene expression analyses was used to characterise the phytoplankton response to different stages of the upwelling cycle. Our results demonstrate that diatoms have an innate ability to 'frontload' nitrogen assimilation, urea cycling and replication system genes during the early stages of an upwelling event. This 'frontloading' occurs even before the increase in biomass and nutrient uptake rate processes is sufficient enough for them to initiate a bloom. We also observed an overall differential expression of genes related to aldolases and ISIPs between diatoms and haptophytes in the context of the upwelling stages, where the constitutive expression of these genes in haptophytes may be contributing to their success in post bloom, nutrient-limited conditions. Conclusively, we postulate that the four stations sampled were not a Lagrangian study tracking the same upwelling plumes, but rather a representation of a series of different stages of upwelling events. We conclude that (1) phytoplankton assemblages at the different stages of upwelling exhibit high molecular and physiological variability given the specific environmental conditions in relation to the particular upwelling water mass; (2) major phytoplankton groups display divergent transcriptional responses that can be distinguished between various stages of early upwelling plumes, but a proactive expression profile can be seen in diatoms; (3) there is an offset between molecular shifts and physiological processes in diatoms during the upwelling cycle,

such that gene expression patterns precede shifts in the environmental conditions around them. This suggests that diatom physiological processes are important indicators to their upwelling response given their innate ability to express key genes and pathways and warrants further investigation.

Potential limitations of our study include the disconnect between metatranscriptomic analyses of distinctive phytoplankton taxa and rate process measurements collected for bulk size-fractionated communities. We therefore assumed that (1) these physiological measurements are representative of all phytoplankton members present and (2) diatoms comprised the majority of the large size fraction, despite many smaller diatoms that can still pass through into the small size fraction. Furthermore, we utilised different upwelling transects to put forth an image of a successive upwelling plume. While this does provide a general picture of early and later upwelling stages, the communities could very well be misrepresented had they been part of the same water mass. Future studies should examine these biological processes through Lagrangian experiments and account for the important physical factors governing coastal upwelling cycles.

Nevertheless, our findings support the concept of phytoplankton differential response to various upwelling stages in the CCS that are crucial to their representation and success in the marine system. Molecular dynamics during the initial upwelling phase drastically differed from that of the later upwelling stages, where the accumulation of biomass coincided with the 'shift-up' response. Given that future oceans are likely to experience changes to the intensity of seasonal upwelling cycles (Benedetti et al. 2021) and increased temperature and acidification of surface waters, these findings can contribute to predictions on the consequences of climate change on primary productivity during these events.

5 | Experimental Procedures

5.1 | Sampling Strategy

Four sites experiencing upwelling (E1: 41° 57.152 latitude, 124° 25.005 longitude. L2: 41° 42.078 latitude, 124° 30.865 longitude. L3: 43° 33.183 latitude, 124° 22.312 longitude. L4: 43° 59.988 latitude, 124° 41.28 longitude) were sampled off the coast of Northern California on May 30, 2019 (E1 and L2) and June 05, 2019 (L3 and L4) aboard the *R/V Oceanus* (Figure 1).

Seawater was collected using a CTD-Rosette sampler at four depths throughout the euphotic zone at each station corresponding to 50%, 30%, 10% and 1% incident irradiance (E1: 5.7, 8.5, 14.5, 26.9 m. L2: 5.7, 9, 16, 27 m. L3 and L4: 5, 7, 14, 27 m). At each depth, samples for size-fractionated chlorophyll *a* (Chl *a*), dissolved inorganic nutrients, size-fractionated dissolved inorganic carbon, and nitrate uptake rates, cell counts and gene expression were obtained. Size fractionation was partitioned between cells greater than or equal to 5 μm or less than 5 μm in diameter. Phytoplankton groups comprising the large size fraction were primarily made up of large diatoms, whereas the small size fraction was primarily made up of non-diatom phytoplankton groups, including haptophytes, chlorophytes and cyanobacteria. Temperature and salinity data were obtained for the upper 75 m of the water column at all four stations, and plotted using R v4.1.0 on Rstudio. Shipboard ADCP measurements were used to assess the speed and direction of currents throughout the water column between station E1 and L2 (Mohn et al. 2018). The ADCP data indicate different flow speeds and directions between station E1 and station L2, although the two stations were formerly thought to be sampled along the same transect. Station E1 also exhibited lower temperatures and a relatively smaller range of salinity relative to L2 and contained the highest macronutrient concentrations of the four stations, while L2 exhibited relatively higher temperatures and the lowest macronutrient concentrations of the four stations. After examining the criteria for all four stations, it was determined that upwelling station E1 depicted the initial onset of an early upwelling plume given its low biomass, high macronutrients, and lower temperature profile. Stations L2, L3 and L4 were grouped based on environmental parameters (TS profiles, higher biomass, lower nutrient concentrations) that were largely different from those of station E1, but also exhibited variability among each other. These stations were categorised as relatively later stations that showed biomass accumulation and increased N assimilation corresponding to that of an early upwelling phase when cells are undergoing enhanced growth rates.

5.2 | Size-Fractionated Chlorophyll a

Approximately 250 mL of seawater was gravity filtered through 5 μm Isopore membrane filters (47 mm) and subsequently filtered onto GF/F (25 mm) filters under 100 mmHg of vacuum perforation. Filters were then rinsed with 0.45 μm filtered seawater and immediately stored at −20°C until onshore analysis in the lab. Chl *a* extraction was performed using a 90% acetone solution kept at −20°C for 24 h until measured on a 10-AU fluorometer (Turner Designs, San Jose, CA) using the acidification method (Parsons et al. 1984).

5.3 | Dissolved Inorganic Nutrients

Nitrogen (nitrate + nitrite), phosphate, and silicic acid concentrations were measured by filtering 30 mL of water through a 0.2 μm filter, using acid-washed syringes into an acid-cleaned polypropylene Falcon tube. Dissolved inorganic nutrient concentrations were analysed using an OI Analytical Flow Solutions IV auto analyser by Wetland Biogeochemistry Analytical Services at Louisiana State University. Concentrations of nitrate measured from the discrete samples were used for the calculation of absolute nitrate uptake rates.

5.4 | Size-Fractionated DIC and NO_3^- Uptake

Seawater from the rosette was collected into polycarbonate bottles (~618 mL) and immediately spiked with both $NaH^{13}CO_3$ and $Na^{15}NO_3$ at approximately 10% of the predicted ambient DIC concentrations and measured nitrate concentrations under a trace metal clean flow hood located on the ship. Samples were then incubated for 6 h and vacuum filtered similarly to Chl *a* measurements, such that cells greater than or equal to 5 μm were

collected onto 5 μm Isopore polycarbonate membrane filters (47 mm), with the flow-through containing cells smaller than 5 μm which were collected onto 0.7 μm pre-combusted GF/F filters. The polycarbonate filters containing cells greater than 5 μm were then rinsed onto new 0.7 μm pre-combusted GF/F filters using 0.45 μm filtered seawater. The filters were then preserved at −20°C until further processing in the laboratory. Prior to analysis, filters were dried at 60°C for 24 h, encapsulated in tin and pelletized. POC, particulate organic nitrogen (PON), and atom percentages of ^{13}C and ^{15}N were subsequently quantified using an isotope ratio mass spectrometer (EA-IRMS) at the UC Davis Stable Isotope Facility. For each sample, POC and PON concentrations (μmol L^{-1}) were calculated by dividing the measured POC/PON mass (μg) by the respective atomic mass of carbon and nitrogen over the volume filtered (0.5 L).

Absolute uptake rates of dissolved inorganic carbon and nitrate (ρ, DIC or NO_3^- taken up per unit time) were derived from the constant transport model (Equation 3 from Dugdale and Wilkerson 1986). The ^{13}C fraction was first calculated by dividing the measured ^{13}C atom percentage in each sample by the natural ^{13}C atom percentage (1.087%), over the difference between the percentage of ^{13}C over total C in the sample and the natural ^{13}C atom percentage. The ^{13}C biomass was then derived by multiplying the ^{13}C fraction by the calculated POC concentration for each sample, and ^{13}C absolute uptake rate was measured as the ^{13}C biomass accumulated over the incubation time (6 h). The same calculations were applied to assess the ^{15}N absolute uptake rates, but with the respective natural atom percentage of ^{15}N (0.367%). Biomass-normalised uptake rates (V, DIC and NO_3^- taken up per unit POC and PON, respectively, per unit time) were derived from the specific uptake model (Equation 6 from Dugdale and Wilkerson 1986), and was assessed by dividing the absolute uptake rates of DIC or NO_3^- by the measured POC and PON concentrations (μmol L^{-1}), respectively.

5.5 | RNA Collection and Extraction

Approximately 2.5 L of seawater from each cubitainer was collected onto 0.8 μm Pall Supor filters (142 mm) using a peristaltic pump, then immediately flash frozen in liquid nitrogen, and stored at −80°C until RNA extraction in the laboratory. RNA was extracted using the RNAqueous-4PCR kit. An additional bead-beating step was added to the extraction procedure, which was followed according to the manufacturer's instructions. The glass beads were used to assist in disrupting cells, particularly those with hard outer coverings (e.g., diatoms). RNA quantity and purity were assessed on a NanoDrop 2000 spectrophotometer (Thermo Fisher Scientific). Library preparation and sequencing of RNA with poly-A tail selection were conducted by GENEWIZ. Sequencing was performed on an Illumina HiSeq 4000 with a 2×150 bp configuration.

5.6 | Metatranscriptome Bioinformatic Pipeline

Reads were trimmed for quality control and adapter removal using Trimmomatic v0.32 (paired-end mode, sliding window of 4:20, and minimum length of 36 bp) and FastQC (Babraham Institute). Trimmed paired reads were then assembled *de novo* into contigs using rnaSPAdes v3.14.1. The assemblies were then clustered using CD-HIT-EST to reduce redundant contigs (Li and Godzik 2006) based on a 98% similarity score, and merged into a mega assembly. Read counts were quantified by mapping trimmed reads to the assembled contigs using SALMON alignment (Patro et al. 2017).

Taxonomic and functional annotations were both performed using the DIAMOND sequencing aligner and its compatible BLASTX command (E-value < 10^{-6}). Taxonomic annotation was identified through phyloDB (v1.076), a custom reference database that also includes sequences from the Marine Microbial Eukaryote Transcriptome Sequencing Project (Keeling et al. 2014). Functional annotation was assigned to contigs using the Kyoto Encyclopedia of Genes and Genomes (Kanehisa et al. 2017). The best hit with a KEGG Ortholog (KO) number from the top hits was selected, and the KEGGANNOT package was used to obtain annotation data for contigs with assigned KOs. Genes of importance without assigned KOs, such as those for the ISIPs and proton-pumping rhodopsin (RHO) were manually added into the subsequent KEGG BLASTX output with a 'pseudo' KO identifier.

Prior to differential expression analysis, read counts were imported and summarised into gene-level estimates for each respective taxonomic group (i.e., diatom, dinoflagellate, chlorophyte, haptophyte) using Tximport (v3.13) (Soneson et al. 2015). Differential expression analysis was performed using DESeq2 (Anders and Huber 2010), and assessed by summing counts of contigs within different taxonomic groups, respectively. The read counts were normalised within each group by the respective transect stations using the 'median ratio method' (Equation 5, Anders and Huber 2010), and dispersions were estimated from replicate samples that were individually sequenced using a negative binomial distribution. Pairwise comparisons of early and later upwelling stages were made by measuring the $\log_2$ fold change of transcripts expressed at E1 relative to the average of transcripts expressed at L2, L3 and L4.

Author Contributions

Study conception and design: Yuan Yu Lin and Adrian Marchetti. Data collection: Yuan Yu Lin, Adrian Marchetti, Olivia Torano, Emily Pierce, Claire P. Till, Matthew Hurst, and Astrid Schnetzer. Analysis and interpretation of results: Yuan Yu Lin, Adrian Marchetti, and Harvey Seim. Draft manuscript preparation: Yuan Yu Lin and Adrian Marchetti.

Acknowledgements

We are grateful for the crew and staff of the R/V Oceanus and their valuable assistance and support throughout the cruise. Funding for the project was provided to A.M. from a National Science Foundation grant (OCE1751805). Trace metal sampling and analysis were funded through C.P.T.'s startup funding through Cal Poly Humboldt as well as the Research Corporation for Science Advancement's Cottrell Scholar Award #26844 to C.P.T.

Ethics Statement

The authors declare adherence to all relevant regulations in sample collection and analysis, reported data with full transparency, and ensured responsible interpretation of the results. In conducting the field component of this research project, we were committed to

minimising disruptions to the natural ecosystems and protected areas of the California Current System and emphasised the importance of avoiding potential harm to all biotic and abiotic entities in the environment.

Conflicts of Interest

The authors declare no conflicts of interest.

Data Availability Statement

Sequence data reported in this study is deposited in the National Center for Biotechnology sequence read archive. RNA sequences are under submission no. SUB13179044 (Bioproject accession no. PRJNA966115).

References

Abbott, M. R., and P. M. Zion. 1987. "Spatial and Temporal Variability of Phytoplankton Pigment Off Northern California During Coastal Ocean Dynamics Experiment 1." *Journal of Geophysical Research: Oceans* 92, no. C2: 1745–1755.

Allen, A. E., C. L. Dupont, M. Oborník, et al. 2011. "Evolution and Metabolic Significance of the Urea Cycle in Photosynthetic Diatoms." *Nature* 473: 203–207.

Anders, S., and W. Huber. 2010. "Differential Expression Analysis for Sequence Count Data." *Genome Biology* 11, no. 10: 1.

Bane, J. M., M. D. Levine, R. M. Samelson, et al. 2005. "Atmospheric Forcing of the Oregon Coastal Ocean During the 2001 Upwelling Season." *Journal of Geophysical Research: Oceans* 110, no. C10: 1–21.

Barber, R. T., and M. R. Hiscock. 2006. "A Rising Tide Lifts All Phytoplankton: Growth Response of Other Phytoplankton Taxa in Diatom-Dominated Blooms." *Global Biogeochemical Cycles* 20: 1–12. https://doi.org/10.1029/2006gb002726.

Barshis, D. J., J. T. Ladner, T. A. Oliver, F. O. Seneca, N. Traylor-Knowles, and S. R. Palumbi. 2013. "Genomic Basis for Coral Resilience to Climate Change." *Proceedings of the National Academy of Sciences of the United States of America* 110: 1387–1392.

Benedetti, F., M. Vogt, U. H. Elizondo, D. Righetti, N. E. Zimmermann, and N. Gruber. 2021. "Author Correction: Major Restructuring of Marine Plankton Assemblages Under Global Warming." *Nature Communications* 12: 6256.

Bernstein, R. L., L. Breaker, and R. Whritner. 1977. "California Current Eddy Formation: Ship, Air, and Satellite Results: Satellite Remote Sensing Combined With Conventional Tools Improves the Ability to Observe Ocean Currents." *Science* 195, no. 4276: 353–359.

Biller, D. V., and K. W. Bruland. 2013. "Sources and Distributions of Mn, Fe, co, Ni, cu, Zn, and cd Relative to Macronutrients Along the Central California Coast During the Spring and Summer Upwelling Season." *Marine Chemistry* 155: 50–70.

Botebol, H., G. Lelandais, C. Six, et al. 2017. "Acclimation of a Low Iron Adapted Ostreococcus Strain to Iron Limitation Through Cell Biomass Lowering." *Scientific Reports* 7: 327.

Bruland, K. W., E. L. Rue, and G. J. Smith. 2001. "Iron and Macronutrients in California Coastal Upwelling Regimes: Implications for Diatom Blooms." *Limnology and Oceanography* 46, no. 7: 1661–1674.

Capone, D. G., and D. A. Hutchins. 2013. "Microbial Biogeochemistry of Coastal Upwelling Regimes in a Changing Ocean." *Nature Geoscience* 6: 711–717.

Checkley, D. M., Jr., and J. A. Barth. 2009. "Patterns and Processes in the California Current System." *Progress in Oceanography* 83, no. 1–4: 49–64.

Cohen, N. R., K. A. Ellis, R. H. Lampe, et al. 2017. "Diatom Transcriptional and Physiological Responses to Changes in Iron Bioavailability Across Ocean Provinces." *Frontiers in Marine Science* 4: 1–20. https://doi.org/10.3389/fmars.2017.00360.

Collos, Y. 1986. "Time-Lag Algal Growth Dynamics: Biological Constraints on Primary Production in Aquatic Environments." *Marine Ecology Progress Series* 33: 193–206.

Collos, Y., A. Vaquer, and P. Souchu. 2005. "Acclimation of Nitrate Uptake by Phytoplankton to High Substrate Levels 1." *Journal of Phycology* 41: 466–478.

Dugdale, R. C., and F. P. Wilkerson. 1986. "The Use of 15N to Measure Nitrogen Uptake in Eutrophic Oceans; Experimental Considerations 1, 2." *Limnology and Oceanography* 31, no. 4: 673–689.

Dugdale, R. C., F. P. Wilkerson, and A. Morel. 1990. "Realization of New Production in Coastal Upwelling Areas: A Means to Compare Relative Performance." *Limnology and Oceanography* 35: 822–829.

Fawcett, S. E., and B. B. Ward. 2011. "Phytoplankton Succession and Nitrogen Utilization During the Development of an Upwelling Bloom." *Marine Ecology Progress Series* 428: 13–31.

Goericke, R. 2011. "The Structure of Marine Phytoplankton Communities-Patterns, Rules and Mechanisms." *California Cooperative Oceanic Fisheries Investigations Reports* 52: 182–197.

Gruber, N., Z. Lachkar, H. Frenzel, et al. 2011. "Eddy-Induced Reduction of Biological Production in Eastern Boundary Upwelling Systems." *Nature Geoscience* 4: 787–792.

Jaubert, M., C. Duchêne, P. G. Kroth, A. Rogato, J.-P. Bouly, and A. Falciatore. 2022. "Sensing and Signalling in Diatom Responses to Abiotic Cues." In *The Molecular Life of Diatoms*, edited by A. Falciatore and T. Mock, 607–639. Springer International Publishing.

Kanehisa, M., M. Furumichi, M. Tanabe, Y. Sato, and K. Morishima. 2017. "KEGG: New Perspectives on Genomes, Pathways, Diseases and Drugs." *Nucleic Acids Research* 45, no. D1: D353–D361.

Keeling, P. J., F. Burki, H. M. Wilcox, et al. 2014. "The Marine Microbial Eukaryote Transcriptome Sequencing Project (MMETSP): Illuminating the Functional Diversity of Eukaryotic Life in the Oceans Through Transcriptome Sequencing." *PLoS Biology* 12, no. 6: e1001889.

Klar, J. K., W. B. Homoky, P. J. Statham, et al. 2017. "Stability of Dissolved and Soluble Fe(II) in Shelf Sediment Pore Waters and Release to an Oxic Water Column." *Biogeochemistry* 135: 49–67.

Kolody, B. C., S. R. Smith, L. Zeigler Allen, et al. 2022. "Nitrogen and Iron Availability Drive Metabolic Remodeling and Natural Selection of Diverse Phytoplankton During Experimental Upwelling." *MSystems* 7: e0072922.

Lampe, R. H., G. Hernandez, Y. Y. Lin, and A. Marchetti. 2021. "Representative Diatom and Coccolithophore Species Exhibit Divergent Responses Throughout Simulated Upwelling Cycles." *MSystems* 6, no. 2: e00188-21.

Lampe, R. H., N. R. Cohen, K. A. Ellis, et al. 2018. "Divergent Gene Expression Among Phytoplankton Taxa in Response to Upwelling." *Environmental Microbiology* 20, no. 8: 3069–3082.

Li, W., and A. Godzik. 2006. "Cd-Hit: A Fast Program for Clustering and Comparing Large Sets of Protein or Nucleotide Sequences." *Bioinformatics* 22, no. 13: 1658–1659.

Lin, Y., O. Torano, L. Whitehouse, et al. 2024. "Variability in the Phytoplankton Response to Upwelling Across an Iron Limitation Mosaic Within the California Current System." *Limnology and Oceanography* 69: 888–901. https://doi.org/10.1002/lno.12534.

Litchman, E., C. A. Klausmeier, O. M. Schofield, and P. G. Falkowski. 2007. "The Role of Functional Traits and Trade-Offs in Structuring Phytoplankton Communities: Scaling From Cellular to Ecosystem Level." *Ecology Letters* 10: 1170–1181.

Marchetti, A., D. M. Schruth, C. A. Durkin, et al. 2012. "Comparative Metatranscriptomics Identifies Molecular Bases for the Physiological

Responses of Phytoplankton to Varying Iron Availability." *Proceedings of the National Academy of Sciences of the United States of America* 109: E317–E325.

Marchetti, A., M. S. Parker, L. P. Moccia, et al. 2009. "Ferritin Is Used for Iron Storage in Bloom-Forming Marine Pennate Diatoms." *Nature* 457: 467–470.

McQuaid, J. B., A. B. Kustka, M. Oborník, et al. 2018. "Carbonate-Sensitive Phytotransferrin Controls High-Affinity Iron Uptake in Diatoms." *Nature* 555: 534–537.

Mohn, C., A. Denda, S. Christiansen, et al. 2018. "Ocean Currents and Acoustic Backscatter Data From Shipboard ADCP Measurements at Three North Atlantic Seamounts Between 2004 and 2015." *Data in Brief* 17: 237–245.

Morrissey, J., R. Sutak, J. Paz-Yepes, et al. 2015. "A Novel Protein, Ubiquitous in Marine Phytoplankton, Concentrates Iron at the Cell Surface and Facilitates Uptake." *Current Biology* 25: 364–371.

Mozetič, P., J. Francé, T. Kogovšek, I. Talaber, and A. Malej. 2012. "Plankton Trends and Community Changes in a Coastal Sea (Northern Adriatic): Bottom-Up vs. Top-Down Control in Relation to Environmental Drivers." *Estuarine, Coastal and Shelf Science* 115: 138–148.

Narimousa, S., and T. Maxworthy. 1985. "Two-Layer Model of Shear-Driven Coastal Upwelling in the Presence of Bottom Topography." *Journal of Fluid Mechanics* 159: 503–531.

Patro, R., G. Duggal, M. I. Love, R. A. Irizarry, and C. Kingsford. 2017. "Salmon Provides Fast and Bias-Aware Quantification of Transcript Expression." *Nature Methods* 14, no. 4: 417–419.

Poulin, F. J., and P. J. S. Franks. 2010. "Size-Structured Planktonic Ecosystems: Constraints, Controls and Assembly Instructions." *Journal of Plankton Research* 32: 1121–1130.

Redfield, A. C., B. H. Ketchum, and F. A. Richards. 1963. "The Influence of Organisms on the Composition of Sea Water." In *The Sea*, edited by M. Hill, 26–77. Interscience.

Rizkallah, M. R., S. Frickenhaus, S. Trimborn, et al. 2020. "Deciphering Patterns of Adaptation and Acclimation in the Transcriptome of *Phaeocystis Antarctica* to Changing Iron Conditions1." *Journal of Phycology* 56: 747–760.

Soneson, C., M. I. Love, and M. D. Robinson. 2015. "Differential Analyses for RNA-Seq: Transcript-Level Estimates Improve Gene-Level Inferences." *F1000Research* 4: 1–23.

Strub, P. T., P. M. Kosro, and A. Huyer. 1991. "The Nature of the Cold Filaments in the California Current System." *Journal of Geophysical Research: Oceans* 96, no. C8: 14743–14768.

Strzepek, R. F., M. T. Maldonado, K. A. Hunter, R. D. Frew, and P. W. Boyd. 2011. "Adaptive Strategies by Southern Ocean Phytoplankton to Lessen Iron Limitation: Uptake of Organically Complexed Iron and Reduced Cellular Iron Requirements." *Limnology and Oceanography* 56: 1983–2002.

Valiela, I. 1984. *Marine Ecological Processes*. Springer.

Van Oostende, N., J. P. Dunne, S. E. Fawcett, and B. B. Ward. 2015. "Phytoplankton Succession Explains Size-Partitioning of New Production Following Upwelling-Induced Blooms." *Journal of Marine Systems* 148: 14–25.

van Tol, H. M., and E. V. Armbrust. 2021. "Genome-Scale Metabolic Model of the Diatom *Thalassiosira pseudonana* Highlights the Importance of Nitrogen and Sulfur Metabolism in Redox Balance." *PLoS One* 16: e0241960.

Wang, X., Y. Wang, and W. O. Smith Jr. 2011. "The Role of Nitrogen on the Growth and Colony Development of *Phaeocystis globosa* (Prymnesiophyceae)." *European Journal of Phycology* 46: 305–314.

Wilkerson, F. P., and R. C. Dugdale. 1987. "The Use of Large Shipboard Barrels and Drifters to Study the Effects of Coastal Upwelling on Phytoplankton Dynamics 1, 2." *Limnology and Oceanography* 32: 368–382.

Supporting Information

Additional supporting information can be found online in the Supporting Information section.